

SparkMaster: automated calcium spark analysis with ImageJ

Eckard Picht, Aleksey V. Zima, Lothar A. Blatter, and Donald M. Bers

Department of Physiology, Stritch School of Medicine, Loyola University Chicago, Maywood, Illinois

Submitted 21 November 2006; accepted in final form 20 March 2007

Picht E, Zima AV, Blatter LA, Bers DM. SparkMaster: automated calcium spark analysis with ImageJ. *Am J Physiol Cell Physiol* 293: C1073–C1081, 2007. First published March 21, 2007; doi:10.1152/ajpcell.00586.2006.—Ca sparks are elementary Ca-release events from intracellular Ca stores that are observed in virtually all types of muscle. Typically, Ca sparks are measured in the line-scan mode with confocal laser-scanning microscopes, yielding two-dimensional images (distance vs. time). The manual analysis of these images is time consuming and prone to errors as well as investigator bias. Therefore, we developed SparkMaster, an automated analysis program that allows rapid and reliable spark analysis. The underlying analysis algorithm is adapted from the threshold-based standard method of spark analysis developed by Cheng et al. (*Biophys J* 76: 606–617, 1999) and is implemented here in the freely available image-processing software ImageJ. SparkMaster offers a graphical user interface through which all analysis parameters and output options are selected. The analysis includes general image parameters (number of detected sparks, spark frequency) and individual spark parameters (amplitude, full width at half-maximum amplitude, full duration at half-maximum amplitude, full width, full duration, time to peak, maximum steepness of spark upstroke, time constant of spark decay). We validated the algorithm using images with synthetic sparks embedded into backgrounds with different signal-to-noise ratios to determine an analysis criteria at which a high sensitivity is combined with a low frequency of false-positive detections. Finally, we applied SparkMaster to analyze experimental data of sparks measured in intact and permeabilized ventricular cardiomyocytes, permeabilized mammalian skeletal muscle, and intact smooth muscle cells. We found that SparkMaster provides a reliable, easy to use, and fast way of analyzing Ca sparks in a wide variety of experimental conditions.

myocytes; sarcoplasmic reticulum; confocal microscopy

CALCIUM SPARKS ARE brief, spatially localized Ca-release events from intracellular Ca stores, triggered by transient openings of a cluster of Ca-release channels (ryanodine receptors). Since their first description in rat ventricular cardiomyocytes (3), Ca sparks have been studied intensely in numerous cell types and experimental conditions, including cardiac muscle (2, 3, 12, 20), skeletal muscle (1, 19), smooth muscle (7, 10), and recently neurons (11). Typically, Ca sparks are measured with Ca-sensitive fluorescent dyes in the line-scan mode with confocal laser-scanning microscopes, yielding two-dimensional images that contain spatial information in one dimension and temporal information in the second dimension. Cytosolic free Ca is represented by different pixel intensities.

The manual analysis of these images is time consuming and prone to errors and is influenced by investigator experience and bias. Therefore, algorithms have been developed that allow automated analysis of sparks in line-scan images. Several extended versions, which originated from a basic analysis

algorithm that only provided the number of events in the analyzed image (4), have been published (9, 14). However, only the program by Cheng et al. (4) is readily available and published with its complete source code. All of these algorithms were implemented as macros using Interactive Data Language (IDL; ITT Visual Information Solutions, CO), which offers an environment for flexible processing and visualization of large data sets. However, the published macros have substantial shortcomings; e.g., no graphical user interface has been implemented so that changes in the analysis parameters have to be made in the source code, images have to be transformed into the TIF format before the analysis, and a licensed IDL installation is required to run the macro.

Therefore, we developed SparkMaster, a program for automated Ca spark analysis in confocal line-scan images, which runs as a plug-in under the freely available image-processing software ImageJ (Wayne Rasband, National Institutes of Health, Bethesda, MD). It is based on the standard algorithm of Ca spark analysis developed by Cheng et al. (4) and provides a graphical user interface in which all analysis parameters and output options can be easily controlled. We extensively validated the analysis parameters using images with synthetic sparks of known properties embedded into backgrounds with different signal-to-noise ratios (SNRs). To test the practicality with experimental data, we used SparkMaster to analyze images obtained in different cellular preparation such as intact and permeabilized ventricular cardiomyocytes, permeabilized mammalian skeletal muscle, and intact smooth muscle cells.

We found that SparkMaster provides a reliable, easy to use, and fast way of analyzing Ca sparks in a wide variety of experimental conditions.

METHODS

Spark analysis algorithm and ImageJ implementation. The spark detection algorithm is derived from the threshold-based algorithm described by Cheng et al. (4) with some modifications. This algorithm was implemented as a Java plug-in into the freely available image-processing software ImageJ. Care was taken to ensure that the results of the ImageJ plug-in would yield the same results as the original IDL macro. A thorough description of the algorithm is provided by Song et al. (17) and by Cheng et al. (4). In short, the algorithm identifies Ca sparks based on their deviation from the background noise. After the image has been low-pass filtered with the use of a 5×5 -pixel median filter and a 4×4 -pixel smoothing filter, it is normalized on a column-by-column basis (i.e., for each position in the line scan). The mean and SD are calculated, and regions exceeding $1.5 \times$ SD are excised to create a point-by-point baseline to normalize the whole image. This normalized image is used for spark detection. Potential sparks are identified as areas exceeding $2 \times$ SD above the mean. The

Address for reprint requests and other correspondence: D. M. Bers, Dept. of Physiology, Loyola Univ. Chicago, Stritch School of Medicine, 2160 South First Ave., Maywood, IL 60153 (e-mail: dbers@lumc.edu).

The costs of publication of this article were defrayed in part by the payment of page charges. The article must therefore be hereby marked “advertisement” in accordance with 18 U.S.C. Section 1734 solely to indicate this fact.

mean and SD are again recalculated without the potential sparks. Finally, sparks are accepted if the area above the 2 SD threshold contains pixel values that exceed the SD multiplied by a threshold factor (*Criteria*, set by the user) plus the background mean. The differences of the SparkMaster algorithm vs. the originally described algorithm are as listed. 1) Sparks are individually analyzed for amplitude (difference between peak spark fluorescence and background fluorescence, $\Delta F/F_0$), full width at half-maximum amplitude (FWHM; μm), full duration at half-maximum amplitude (FDHM; ms), full width (μm), full duration (ms), time-to-peak (ms), maximum steepness of spark upstroke, and exponential time constant of the spark decay (ms). 2) An individual input image can be divided into up to five separate segments. The noise level is then determined separately for each segment, allowing more accurate event detection if the noise level changes during data acquisition. When the user sets the number of intervals to one, the plug-in works like the original macro. 3) Events that are completely contained in the region of a previously detected spark are not considered separate sparks. 4) Long-lasting Ca-release events can be analyzed. 5) Multiple images can be analyzed with the same analysis settings. 6) Some problems that caused the original IDL macro to function improperly were resolved. A flow diagram of the algorithm is shown in Fig. 1.

Installation and usage. A working installation of ImageJ is required to run SparkMaster. ImageJ is in the public domain and can be downloaded from the ImageJ website (<http://rsb.info.nih.gov/ij/>). Because ImageJ runs platform independent, SparkMaster can be used with any Windows, Macintosh, or Linux operating system. To install SparkMaster, the file "SparkMaster_.class" has to be copied into the "plugins" subfolder of the ImageJ installation. (The online version of this article contains supplemental data, in which the SparkMaster_.class file is available for download.) Updated versions will be posted on <http://sparkmasterhome.googlepages.com>. After

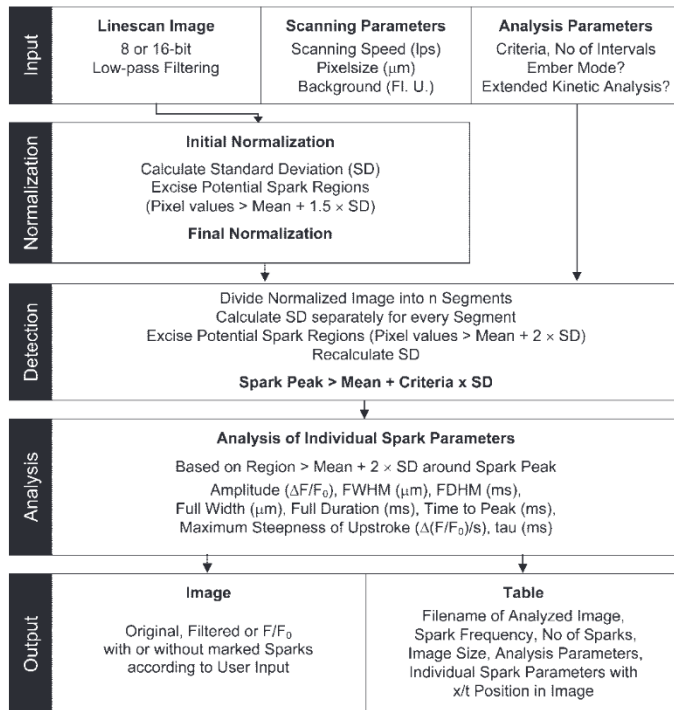


Fig. 1. Flow diagram of the analysis algorithm. The currently active image in ImageJ is analyzed by SparkMaster. Scanning and analysis parameters are selected via the graphical user interface. All of the following steps are performed automatically. $\Delta F/F_0$, amplitude; FWHM, full width at half-maximum amplitude; FDHM, full duration at half-maximum amplitude; Fl U, fluorescence units; lps, lines per second.

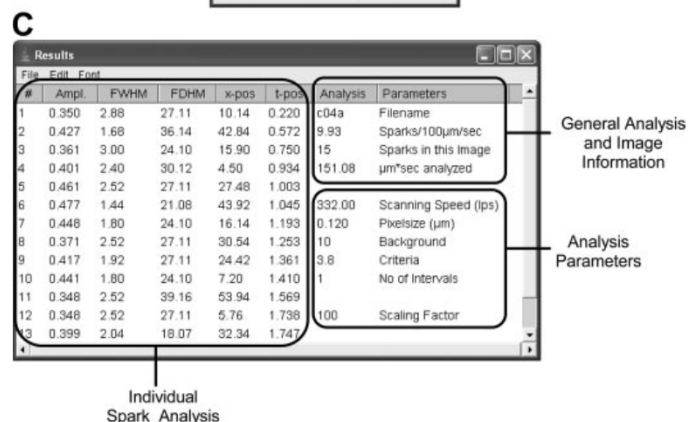
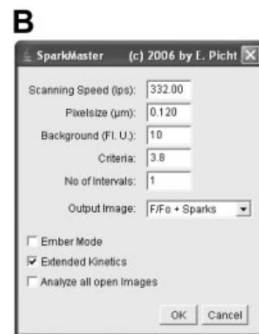
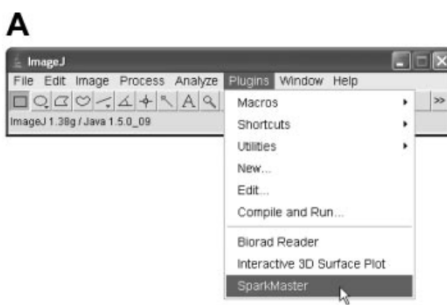


Fig. 2. Implementation of SparkMaster into ImageJ. A: after installation, SparkMaster is listed as an option in the plugins menu. An active image is required to start SparkMaster. B: SparkMaster graphical user interface. C: output data table with analysis of individual sparks on left, general analysis and image information on top right, and analysis parameters on bottom right.

ImageJ is restarted, SparkMaster appears as an option in the plugins menu of ImageJ (Fig. 2A). To start SparkMaster, an image has to be open (both 8-bit and 16-bit images can be analyzed). Some microscopes (e.g., Leica and Olympus) save the acquired images as TIF files, which can be directly opened with ImageJ. Images acquired with Bio-Rad or Zeiss microscopes can be imported into ImageJ using the Bio-Rad Reader and LSM Reader plugins, respectively. For analysis, the spatial dimension of the line-scan image has to be horizontal and the temporal dimension has to be vertical (time progressing from top to bottom). After the SparkMaster option in the plug-ins menu is selected, the SparkMaster graphical user interface appears (Fig. 2B).

The following parameters have to be adjusted before the analysis: *Scanning Speed* (in lines per second) and *Pixel size* (μm) according to the microscope settings during the experiment and *Background* (in fluorescence units) according to the level of noncellular background fluorescence in the acquired image. Regions where the fluorescence in the data image is below the determined noncellular background level are excluded from the analysis (this case occurs when part of the scan line is positioned outside of the cell margins). Please note that the *Background* value is not used for background subtraction. *Criteria*

determines the threshold factor for the detection of sparks above the noise level of the image. Based on the validation, we recommend *Criteria* = 3.8; i.e., the threshold for the detection of events is 3.8 times the SD of the background noise over the mean value of the background. Using this setting, the algorithm shows a high sensitivity and a very low frequency of false-positive detections (for more details on the performance of the algorithm, see below). In case the noise level changes during the image acquisition, the image can be analyzed in several evenly sized segments for which the background noise is calculated separately (*Number of Intervals*, maximum of 5).

The *Ember Mode* option allows the analysis of long-lasting Ca-release events (up to 2.5 s). Such events can occur in mammalian skeletal muscle as embers (22), but they can also occur under certain conditions in cardiomyocytes (13, 21, 23). Because the analysis in *Ember Mode* is more time consuming, we recommend that this option should be disabled when no long-lasting release events are present.

A more comprehensive analysis of individual spark kinetics can be performed when the *Extended Kinetics* option is enabled. In addition to the basic kinetic parameters (amplitude, FWHM, FDHM), individual sparks are also analyzed for full width, full duration, time to peak, maximum steepness of the upstroke, and time constant of the spark decay. Full duration is a useful parameter for the quantification of long-lasting sarcoplasmic reticulum (SR) Ca-release events whose fluorescence may decay below the half-maximum fluorescence after the peak and continue at this low level for a substantial amount of time. The maximum steepness of the spark upstroke is a measure for the maximal SR Ca-release flux underlying the spark (16), and the time to peak can be used as a measure for the duration of the Ca release (18). The exponential time constant of the spark decay, on the other hand, provides insight into Ca buffering as well as SR Ca uptake (5).

When the *Analyze All Open Images* option is activated, all images that are open in ImageJ will be analyzed with the same analysis settings. This option is useful to analyze a large number of images that were obtained under the same experimental conditions.

The analysis is started by clicking the “OK” button. The analysis output consists of two parts. The first part is a data table showing the analysis of individual sparks, general analysis, and information about the analyzed image [file name, spark frequency in events·100 μm⁻¹·s⁻¹, total number of detected sparks, and the image size (in μm × s)] and the analysis parameters (Fig. 2C). If several images were analyzed with the *Analyze All Open Images* option, a single results data table will be generated containing the results from all analyzed images. This table can either be saved by the “File/Save As” command or can be copied into the clipboard (using the “Edit/Copy” command) and then imported or pasted into any other program for further analysis.

The second part of the analysis is the *Output Image*, whose appearance can be selected via the user interface. Options are *Raw* (input image remains unchanged), *Filtered* (input image is shown after filtering), and *F/F₀* (a scaled *F/F₀* image is shown, with the scaling factor listed in the data table). If an option is chosen with the extension + *Sparks*, detected spark regions are marked and numbered corresponding to the labeling in the output data table. The *Output Image* selection has no effect on the analysis; it solely influences the display of the analysis. The *Output Image* can be saved with the use of ImageJ’s built-in commands and further processed, e.g., for pseudocolor transformation or three-dimensional visualization.

The analysis parameters (Fig. 2B) are saved automatically and do not have to be readjusted when a new image is analyzed with the same settings.

Generation of images containing synthetic sparks and validation process. Simulated sparks following the shape of experimentally obtained sparks were generated with ImageJ and inserted into backgrounds of defined Gaussian noise. The amplitudes of the simulated sparks ranged from 0.05 to 0.79 ΔF/F₀; all backgrounds had the same mean value of 38 with SD of 19, 12.6, and 9.5 [equivalent to SNR

(defined as mean/SD) of 2.0, 3.0, and 4.0]. We typically observed an SNR of ~3 in both intact and permeabilized cardiomyocytes; however, under certain experimental conditions or with different microscopes, the noise level might be higher or lower. The noise levels of the test images therefore realistically represent experimental conditions. Each image contained 16 identical synthetic sparks randomly distributed into a background image of 512 × 1,024 pixels (corresponding to an image width of 61.44 μm and a scanning duration of 3.08 s at a pixel size of 0.12 μm and a scanning speed of 332 lines/s; these settings reflect our typical experimental conditions). The event frequency was therefore 8.44 sparks·100 μm⁻¹·s⁻¹ and thus similar to the typically obtained spark frequency in permeabilized cat ventricular myocytes under control conditions (see RESULTS, *Analysis of experimentally obtained Ca sparks*). For each spark amplitude at a given background, 10 images with different spark positions were analyzed with analysis *Criteria* ranging from 3.0 to 4.0. Each data point in Fig. 4 represents the average of 10 analyzed images (error bars omitted for clarity), which were fitted with a Hill function with variable slope.

Figure 3A shows an excerpt of a test image containing 10 randomly distributed simulated sparks with amplitudes of 0.45 ΔF/F₀. Figure 3B shows the same sparks embedded into Gaussian noise with an SNR of 3.0. Figure 3C shows the image after analysis (*Output Image* option: *F/F₀ + Sparks*). Detected spark regions are clearly marked and chronologically numbered (from top to bottom) corresponding to the analysis of individual sparks in the output table. True-positive and false-positive detected events were determined by comparison of the detected events with the position of the originally inserted synthetic sparks.

Measurement of Ca sparks in intact and permeabilized ventricular cardiomyocytes. Cat ventricular myocytes were isolated as previously described (25). Animals of either sex were anesthetized with thiopental sodium (30 mg/kg ip). After thoracotomy, hearts were quickly excised, mounted on a Langendorff apparatus, and perfused with collagenase-containing solution at 37°C. All procedures were performed in accordance with the *Guide for the Care and Use of Laboratory Animals* and were approved by the Institutional Animal Care and Use Committee.

For spark measurements in intact cardiomyocytes, cells were loaded with the Ca indicator fluo 4 by 20-min incubation in Tyrode solution containing 10 μmol/l fluo 4-AM (Invitrogen) at room temperature. Cells were then plated on laminin-coated coverslips and superfused for 20 min with normal Tyrode solution to allow deesterification. The Tyrode solution consisted of (in mM) 140 NaCl, 4 KCl, 2 CaCl₂, 1 MgCl₂, 10 glucose, and 5 HEPES, pH adjusted to 7.4 with NaOH. Because cat ventricular myocytes experience a gradual decrease in SR Ca load under resting conditions (rest decay), cells were field stimulated at 1 Hz in the presence of 1 μmol/l isoproterenol to increase SR Ca load. Sparks were measured within 30 s after the termination of electrical stimulation.

Spark measurements in permeabilized cardiomyocytes were performed after saponin permeabilization. First, the cells were suspended in a solution containing (in mM) 100 potassium aspartate, 20 KCl, 0.5 EGTA, 0.75 MgCl₂, and 10 HEPES (pH adjusted to 7.2 with KOH) and placed in the experimental chamber (final volume = 50 μl) for 15 min. The cell surface membrane was permeabilized by addition of 0.005% (wt/vol) saponin for 30 s. After 30 s, the bath solution was exchanged to a saponin-free internal solution composed of (in mM) 100 potassium aspartate, 15 KCl, 5 KH₂PO₄, 5 MgATP, 0.35 EGTA, 0.14 CaCl₂, 0.75 MgCl₂, 10 phosphocreatine, and 10 HEPES, as well as 5 U/ml creatine phosphokinase, 8% dextran (relative molecular weight = 40,000), and 0.04 mM fluo 4 pentapotassium salt (Invitrogen), pH 7.2 with KOH. Free Ca and Mg concentrations of this solution were 150 nM and 1 mM, respectively (calculated with WinMAXC 2.05, Stanford University).

Ca sparks were recorded with a confocal laser-scanning microscope in the line-scan mode with the scanning line placed parallel to

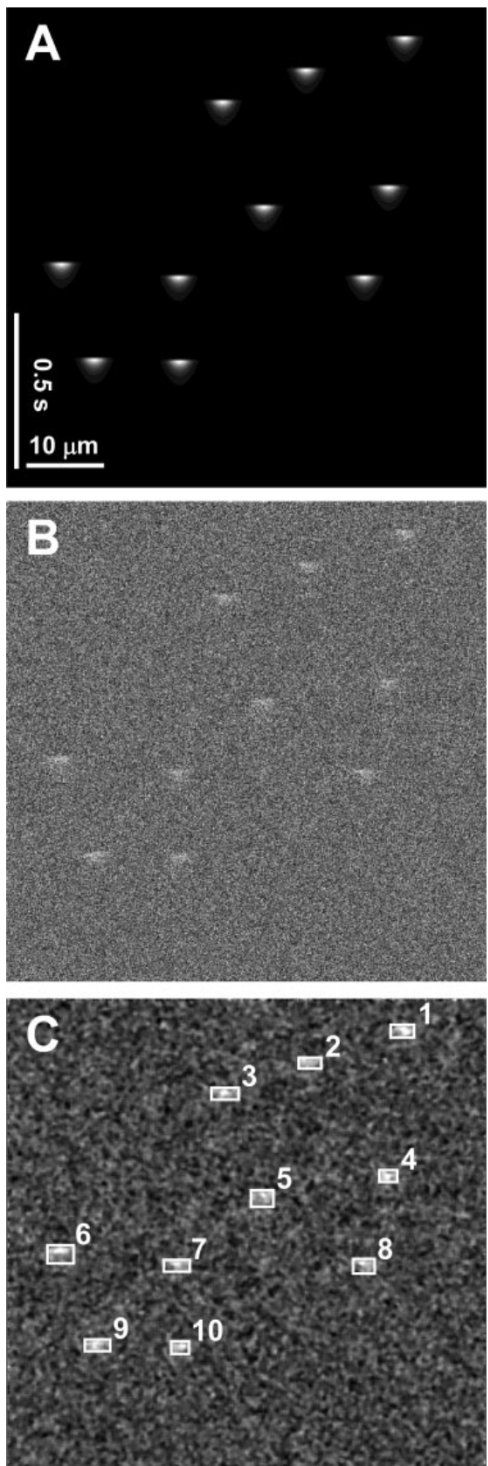


Fig. 3. Generation and analysis of images with synthetic sparks. *A*: synthetic sparks in noise-free background. *B*: synthetic sparks embedded into a background of signal-to-noise ratio (SNR) = 3.0. *C*: analyzed image (*Output Image* option $F/F_0 + \text{Sparks}$). Detected events are marked and labeled.

the longitudinal axis of the cell at a central focal plane (Radiance 2000/MP, Bio-Rad; scanning speed 332 lines/s, pixel size = 0.12 μm). Fluo 4 was excited with the 488-nm line of an argon ion laser, and fluorescence was measured at wavelengths >515 nm. All experiments were performed at room temperature.

Measurement of Ca sparks in skeletal and smooth muscle cells. Images of Ca sparks measured in permeabilized mouse skeletal [extensor digitorum longus (EDL)] muscle were kindly provided by Dr. Vyacheslav M. Shkryl and Dr. Natalia Shirokova (University of Medicine and Dentistry of New Jersey, New Jersey Medical School, Newark, NJ). Animal procedures were similar to those described previously (8, 15), in accordance with the *Guide for the Care and Use of Laboratory Animals* and approved by the Institutional Animal Care and Use Committee at New Jersey Medical School. The EGTA-buffered internal solution was as described previously (15), with L-aspartate substituting for L-glutamate in equimolar amounts.

Images of Ca sparks measured in intact rabbit portal vein smooth muscle cells were kindly provided by Dr. Maksym Harhun and Dr. Thomas B. Bolton (St. George's Hospital Medical School, London, UK). Animal procedures were as described before (6, 7) and approved under Schedule 1 of the UK Animals (Scientific Procedures) Act of 1986. Recording conditions were as described before (6, 7).

RESULTS

Validation of analysis algorithm. The results of the sensitivity analysis are shown in Fig. 4. This analysis was performed with synthetic sparks ranging in amplitude from 0.05 to 0.79 $\Delta F/F_0$ at SNRs from 2.0 to 4.0 using detection *Criteria* from 3.0 to 4.0. Sensitivity (i.e., the true positive rate) is defined as the probability that the program detects an event at a position in the test image where a synthetic event is embedded.

As expected, the sensitivity of the analysis increases with increased spark amplitude and increased SNR. At high noise levels (e.g., SNR 2.0, Fig. 4Aa), the sensitivity increases gradually with increased spark amplitude leading to a wide range of spark amplitudes where only a fraction of sparks is correctly detected. At lower noise levels (e.g., SNR 3.0, Fig. 4Ab; SNR 4.0, Fig. 4Ac), the range of partial spark detection occurs at lower amplitudes and over a narrower range (i.e., the sensitivity curves are shifted to the left, are steeper, and clustered over a narrower range). The spark amplitudes at which the algorithm identifies 90% of Ca sparks using *Criteria* = 3.8 are indicated in Fig. 4A. The relationship between *Criteria* and amplitude at which 90% detection is achieved is shown for SNRs of 2.0, 3.0, and 4.0 in Fig. 4Ba; 90% detection occurs at lower amplitudes as the threshold *Criteria* is decreased. However, decreasing *Criteria* to attain higher detectability can also increase false positives (see next paragraph). Of course, higher SNR allows detection of smaller events for all *Criteria*. The steepness of the sensitivity curves is more strongly influenced by SNR than by *Criteria* (Fig. 4Bb). However, with a low SNR, the low steepness (Fig. 4Aa) indicates that the amplitude range at which only a fraction of sparks is correctly detected is very broad.

Although detectability can be enhanced by decreasing the analysis *Criteria* (sensitivity curves shift to the left), this comes at the price of an increased rate of false-positive detections, especially when the SNR is low (i.e., events are detected where no synthetic sparks exist in the test image). This effect is shown in Fig. 4Bc where the frequency of false positive detections is shown as a function of the threshold *Criteria* at different SNRs. The detection of false-positive events is largely independent of the amplitude of the embedded synthetic sparks when a *Criteria* larger than 3.2 is used. Surprisingly, when a *Criteria* between 3.1 and 3.4 is used, the frequency of false-positive detections is slightly higher at lower noise levels of the input image. However, at the noise

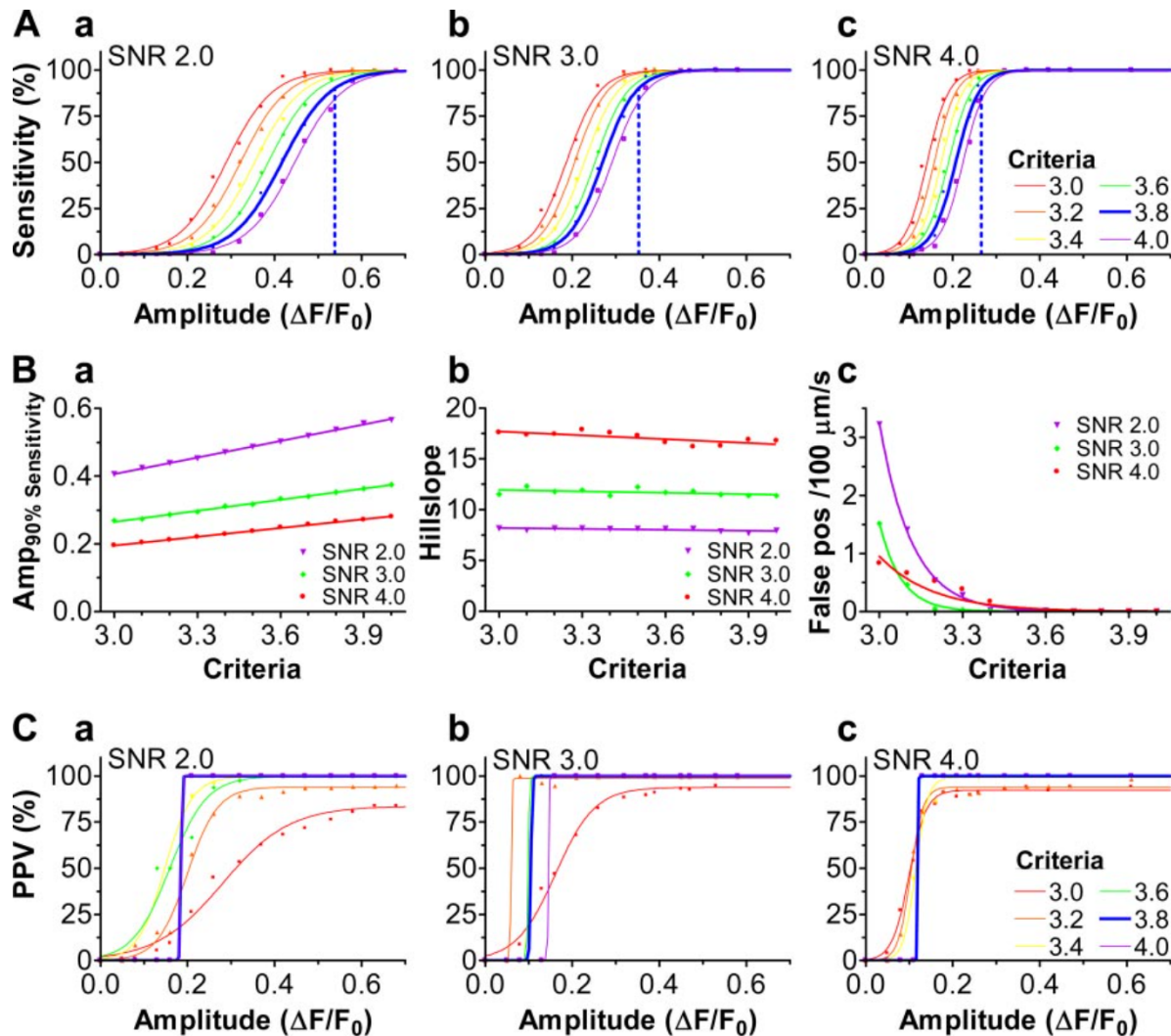


Fig. 4. Performance analysis and positive predictive value (PPV) of the detection algorithm. *A*: sensitivity analysis at SNRs of 2.0 (*a*), 3.0 (*b*), and 4.0 (*c*). Vertical dashed lines show the spark amplitude at which the algorithm operates with 90% sensitivity using *Criteria* = 3.8. *Ba*: amplitude at which 90% sensitivity is attained (Amp_{90% sensitivity}) as a function of *Criteria* at SNRs of 2.0, 3.0, and 4.0. *Bb*: steepness of the sensitivity curves (represented as Hill slope of the curve fits in Fig. 4*A*) as a function of threshold *Criteria*. Steep slopes indicate a sharp transition from low to high sensitivity. *Bc*: frequency of false-positive (pos) detections at different SNRs. *C*: PPV of the analysis as a function of amplitudes for SNRs of 2.0, 3.0, and 4.0.

levels tested here, no false-positive events are detected in the synthetic spark images when a *Criteria* of 3.8 or higher is used.

The positive predictive value of the analysis [PPV; number of true positives/(number of true positives + number of false positives), representing the probability that a detected event is indeed a spark] is shown as a function of spark amplitudes in Fig. 4*C*. Detection *Criteria* ranged from 3.0 to 4.0, and the SNR ranged from 2.0 to 4.0. For low threshold *Criteria* (<3.2), the PPV is always below 100% even with high spark amplitudes and low noise levels. The reason for this is that, despite the high sensitivity at low *Criteria* [sensitivity curves shift to the left (Fig. 4*A*) and detectability of small events is high (Fig. 4*Ba*)], false-positive detections are more likely (Fig. 4*Bc*). However, with threshold *Criteria* = 3.8 and higher, the PPV attains 100% at spark amplitudes between 0.1 and 0.2 $\Delta F/F_0$ at the noise levels tested here. Overall, *Criteria* of 3.8 appears nearly optimal for the Ca sparks and conditions simulated here, although events with amplitudes <0.1 $\Delta F/F_0$ are not detected at this *Criteria*.

Analysis of experimentally obtained Ca sparks. To test the practicability of SparkMaster with original experimental data and to show how individual spark parameters can be used for further analysis, we analyzed Ca sparks that were measured in different cellular preparations: intact and permeabilized cat ventricular myocytes, permeabilized mouse skeletal (EDL) muscle, and intact rabbit portal vein smooth muscle cells. The analysis was performed with the raw images, and no background subtraction was performed.

Images obtained in intact and permeabilized cat ventricular myocytes were analyzed using *Criteria* of 3.4, 3.6, and 3.8 to investigate how the validation results obtained with simulated sparks can be applied to experimental data. Excerpts of typical raw images are shown in Fig. 5*Aa* (sparks in intact cardiomyocytes) and 5*Ba* (sparks in permeabilized cardiomyocytes). Figure 5, *Ab* and *Bb*, shows the normalized images (*Output Image*: F/F_0) after analysis. The normalization removed the vertical lines noticeable in the raw images, and filtering by the algorithm resulted in a substantial decrease of the background

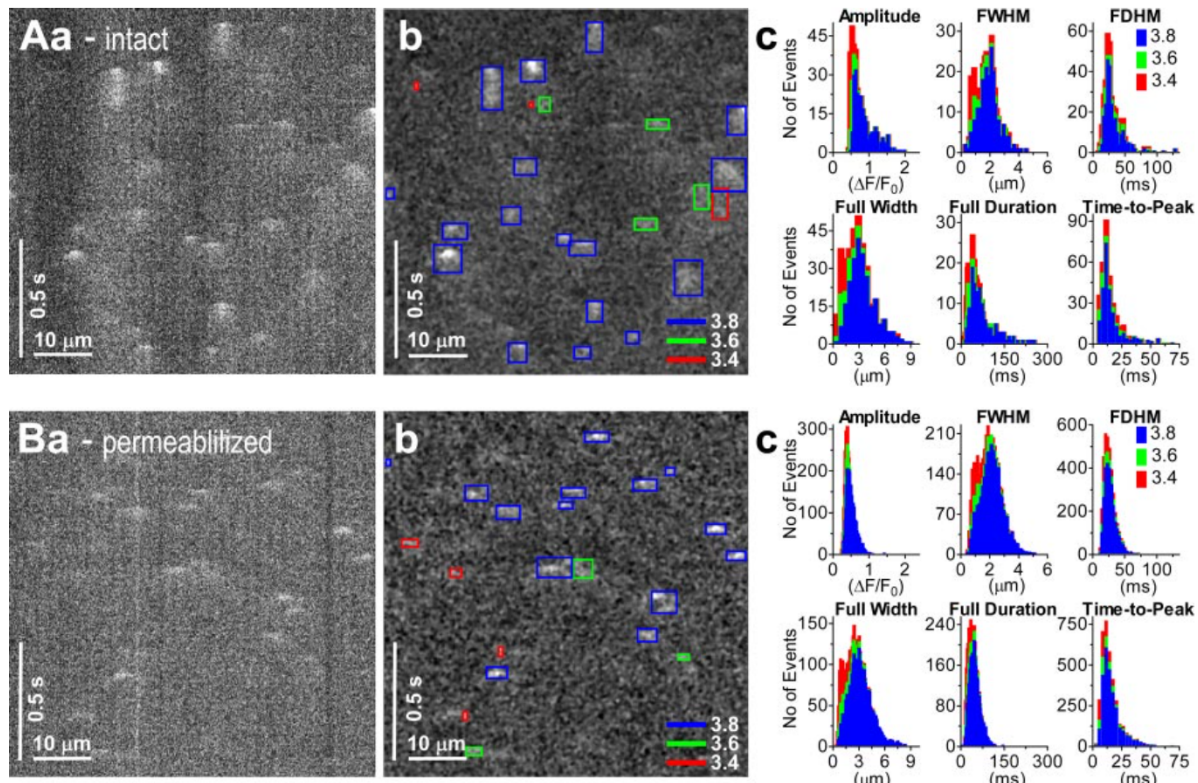


Fig. 5. Analysis of Ca sparks in cardiac muscle. *Aa*: excerpt of a line-scan image obtained in an intact cat ventricular myocyte. *Ab*: F/F_0 image of the same region shown in *Aa*. Detected events are marked in blue (using *Criteria* = 3.8), green (additionally detected events with *Criteria* = 3.6), and red (additionally detected events with *Criteria* = 3.4). *Ac*: histograms of individual spark parameters. Twelve images were analyzed in which 359, 298, and 256 sparks were detected with *Criteria* = 3.4, 3.6, and 3.8, respectively. *Ba*: line-scan image of Ca sparks in permeabilized cat ventricular cardiomyocytes. *Bb*: F/F_0 image with marked detected events. Colors are as described above. *Bc*: histograms of individual spark parameters; 135 images were analyzed in which 3,699, 3,123, and 2,727 sparks were detected with *Criteria* = 3.4, 3.6, and 3.8, respectively.

noise. To illustrate the different performances of the algorithm when using these *Criteria*, the detected events are marked with a blue box when detected at *Criteria* = 3.8; additional events detected with *Criteria* = 3.6 and 3.4 are marked in green and red, respectively. All of the events that are detected with *Criteria* = 3.8 (blue boxes in Fig. 5, *Ab* and *Bb*) have a clear correlate in the raw image. Similar to the images with simulated sparks, smaller *Criteria* led to the additional detection of events with small amplitudes. A correlate in the raw image for the additionally detected events using *Criteria* = 3.6 or 3.4 is far less distinct, and these events are probably at least in part false-positive detections.

The histograms in Fig. 5, *Ac* and *Bc*, summarize the kinetic analysis of individual sparks measured in intact and permeabilized myocytes, respectively. As additional events are detected at lower threshold *Criteria*, the calculated spark frequency increases. The apparent spark frequency was highest with *Criteria* = 3.4 (10.28 ± 1.34 and 11.51 ± 0.74 sparks $\cdot 100 \mu\text{m}^{-1} \cdot \text{s}^{-1}$ in intact and permeabilized myocytes, respectively), decreased by $\sim 16\%$ at *Criteria* = 3.6, and decreased further by $\sim 15\%$ when *Criteria* = 3.8 was used (spark frequency of 8.22 ± 1.15 and 7.57 ± 0.6 sparks $\cdot 100 \mu\text{m}^{-1} \cdot \text{s}^{-1}$ in intact and permeabilized myocytes, respectively). Because the number of detected events with smaller amplitudes increases at lower *Criteria*, the average spark amplitude decreases accordingly (average amplitude of all detected events in intact myocytes was 0.802, 0.857, and 0.905 $\Delta F/F_0$ and in permeabilized

myocytes 0.495, 0.520, and 0.539 $\Delta F/F_0$ using *Criteria* = 3.4, 3.6, and 3.8, respectively). Furthermore, additionally detected events are typically narrow (small FWHM and small full width), show a small full duration, but have a similar FDHM and time to peak.

Properties of sparks measured in intact and permeabilized myocytes were very similar (Fig. 5, *Ac* and *Bc*), but amplitudes were higher in intact cells. All other analyzed parameters (FWHM, FDHM, full width, full duration, and time to peak) were comparable for both conditions.

Next, we analyzed Ca sparks in line-scan images that were measured in permeabilized mouse skeletal (EDL) muscle under conditions described previously (8, 15). The analysis was performed with *Criteria* = 3.8; because the background fluorescence slightly decreased during the acquisition (probably due to photobleaching of compartmentalized dye), we chose “5” for *Number of Intervals*. Additionally, the analysis was done in *Ember Mode* to correctly analyze prolonged Ca-release events. A raw line-scan image is shown in Fig. 6A; Fig. 6B shows the normalized image ($F/F_0 + \text{Sparks}$) after analysis. Figure 6C shows the histograms of the kinetic parameters of the detected sparks. Compared with the sparks measured in cardiomyocytes, sparks in skeletal muscle show similar amplitudes and spatial spread but substantially longer durations. Both the histograms of the FDHM and of the full duration are skewed to longer values; typical examples are events 5 and 11 in Fig. 6D, which are also shown in profile in Fig. 6D. In Fig.

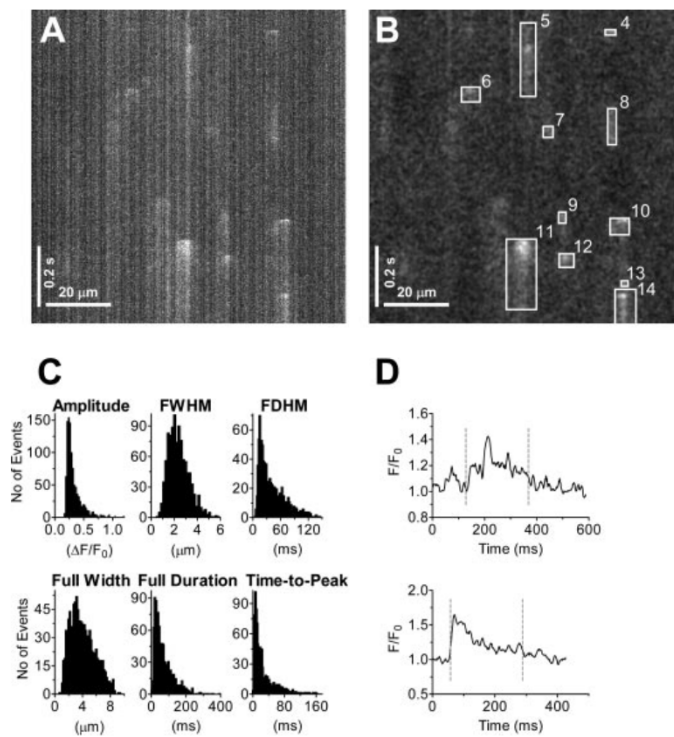


Fig. 6. Ca sparks in skeletal muscle. *A*: raw line-scan image of sparks recorded in permeabilized mouse extensor digitorum longus muscle. *B*: normalized image with marked sparks after analysis using *Criteria = 3.8* (*Output Image* option $F/F_0 + \text{Sparks}$). *C*: histograms of individual spark properties. Histograms are based on 1,035 events detected in 100 images using a *Criteria* of 3.8. *D*: profile plots of spark 5 (top) and spark 11 (bottom) averaged over 5 pixels. Dashed lines indicate detected beginning and ending of events. Raw images were kindly provided by Dr. Vyacheslav M. Shkryl and Dr. Natalia Shirokova (Department of Pharmacology and Physiology, New Jersey Medical School).

6*D*, the detected beginning and ending of the spark are indicated. The profile of spark 5 shows that the full duration can be a valuable parameter and a better index for the duration of the spark than the FDHM.

We finally used SparkMaster to analyze Ca sparks measured in rabbit portal vein myocytes as described before (7). Figure 7*A* shows a representative raw image, Fig. 7*B* shows the F/F_0 image after analysis (*Output Image*: $F/F_0 + \text{Sparks}$), and Fig. 7*C* shows the profile plot of the region marked by the black box to the left of the F/F_0 image. The detected maximum steepness of the spark upstroke and the exponential fit of the spark decay are also indicated. Because the noise level in the raw image is low and the amplitude of events is relatively high, the analysis was performed with *Criteria = 3.2*. Amplitudes, kinetics, and spatial spread of Ca-release events varied substantially even when initiating at the same site. Therefore, elementary Ca-release events in smooth muscle can be grouped into small and large events (6). The automated analysis with SparkMaster largely reproduced the previously described results (6): the origin of the release events varied by a maximum of 0.8 μm (determined from x-pos in analysis data table; see Fig. 2*C*), confirming that all release events shown in Fig. 7 initiate at the same release site. The time to peak was slightly shorter in the small events (events 2, 4, and 7 in Fig. 7*B*), but the average values for the maximum steepness of the upstroke were substantially higher

in the large events than in the small events [106 vs. 60 $\Delta(F/F_0)/\text{s}$; Fig. 7*C*]. Differences in the spatial spread between large and small events are especially prominent when the full width and full duration are used to describe these events (average full width was 10.5 and 5.5 μm in small and large events, respectively; average full duration was 83.6 ms in large and 38.6 ms in small events). The declining phase of the small events was well fitted by SparkMaster with a single exponential function (average time constant = 19.7 ms). Although large events are best fitted with the sum of two exponential functions (6), the results obtained from the SparkMaster analysis resemble very closely the fast component of the decline [average time constant obtained with SparkMaster was 42.2 ms, whereas the fast time constant described by Gordienko and Bolton (6) was 37.6 ms]. The close match of the automatically analyzed parameters with the original profile plot shows the high level of accuracy that the analysis algorithm can achieve.

DISCUSSION

Ca sparks are routinely measured in all types of muscle to study the regulation of Ca release from intracellular stores. Spark frequency and characteristics of individual Ca sparks change in response to physiological cellular alterations (e.g., Ca load of intracellular stores, cytosolic Ca concentration, ryanodine receptor phosphorylation state). Ca sparks are typically measured in line-scan mode with confocal laser-scanning microscopes. Because manual spark analysis is impractical, several automated algorithms have been developed that allow automated Ca spark analysis in line-scan images (4, 9, 14). The algorithm developed by Cheng et al. (4), which detects sparks based on whether the signal exceeds a certain threshold over the background noise level, has become the most widely used algorithm for automated spark detection. However, so far, this algorithm is only available as an IDL macro, which is not

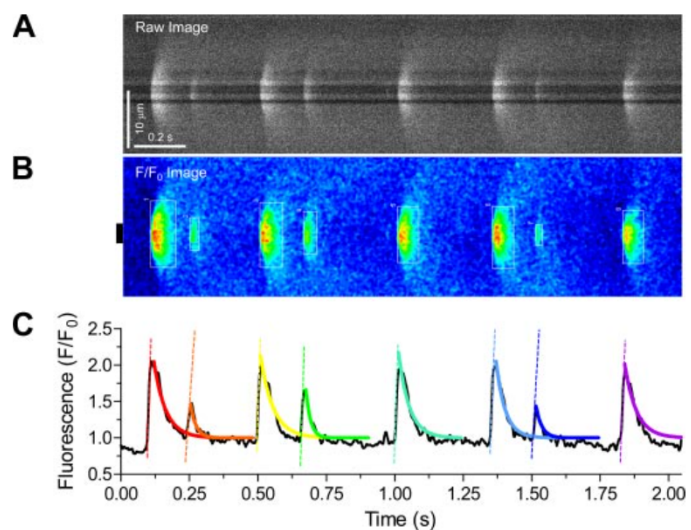


Fig. 7. Ca sparks in smooth muscle (rabbit portal vein myocytes). *A*: raw image. *B*: *Output Image* option $F/F_0 + \text{Sparks}$. *C*: profile plot of the *Output Image* from the region marked with the black box (*B*, left). Dashed lines and solid curves in the profile plot were drawn using the values for the maximal steepness of the spark upstroke and the time constant of the spark decay, as calculated by the SparkMaster program. Raw images were kindly provided by Dr. Maksym Harhun and Dr. Thomas B. Bolton (St. George's Hospital, London, UK).

optimized for user-friendly application. We therefore aimed to develop a user-friendly automated Ca spark analysis program based on the most widely accepted algorithm published so far.

For several reasons, we decided to use the image-processing software ImageJ as an environment to implement our spark detection program; ImageJ is freely available over the Internet and can therefore be installed without costly software licensing on as many computers as needed. It is standard software in the imaging community, and most people working with confocal microscopes are already familiar with this program. Finally, extensions to ImageJ's built-in commands can easily be implemented as Java classes and run as plug-ins. Therefore, the SparkMaster plug-in should find wide utility because it is based on the gold standard of spark analysis, is much easier to use than the original IDL macro, and runs in an already accepted environment.

We intentionally did not include an option that allows the user to manually remove seemingly false-positive-detected events. It has been shown that these manual interventions induce false modes into the spark amplitude histograms because of the preferable rejection of sparks with small amplitudes (17).

Because no analysis exists that can analyze spark data with perfect sensitivity and specificity, we generated images with synthetic Ca sparks of known properties and embedded these into backgrounds with defined Gaussian noise. The comparison between the synthetic images and the analysis results allowed us to validate the analysis algorithm and to determine an optimal threshold criteria. The event frequency and the range of background noise in the test images were comparable to typical experimental images from different cellular preparations that we subsequently used to test the SparkMaster program. However, the situation with experimentally obtained images may be more complex because the background noise level is often inhomogeneous, which can hamper the ability of the algorithm to correctly identify release events. The sensitivity of the analysis is influenced both by the SNR of the raw image and by the threshold *Criteria* with which the analysis is performed. The effect of the *Criteria* on the sensitivity is most prominent at low SNRs (evident by the larger shift of the sensitivity curves in response to altered *Criteria* at low SNR; Fig. 4A). However, decreasing the threshold *Criteria* in an attempt to increase the sensitivity leads to an increased frequency of false-positive detections, especially in noisy images (Fig. 4Bc). From the analysis shown in Fig. 4B, it becomes clear that finding experimental settings that allow data acquisition with a high SNR is a better strategy to achieve a high sensitivity than decreasing the threshold *Criteria*. With the noise levels tested here, a *Criteria* = 3.8 allows the algorithm to detect sparks with a high sensitivity and a very low frequency of false-positive detections. Combined, this leads to a very high PPV in the simulated images at spark amplitudes of $>0.15 \Delta F/F_0$.

Finally, we tested the practicability of SparkMaster with experimental data obtained in different cellular preparations: intact and permeabilized cat ventricular myocytes, mouse permeabilized skeletal (EDL) muscle, and intact rabbit portal vein smooth muscle cells. Images obtained in intact and permeabilized ventricular myocytes were analyzed with threshold *Criteria* = 3.4, 3.6, and 3.8. Similar to the synthetic spark images used for the validation, analyzing images with a lower

Criteria leads to the additional detection of events with small amplitudes and small spatial spread. However, it is not possible to determine how many of the additionally detected events at lower *Criteria* are real sparks and how many are false-positive detections. A *Criteria* of 3.8, which led to a high sensitivity and a low number of false-positive detection in simulated images, can be used as a reasonable starting value for the analysis, which can then be adjusted depending on the background noise level, amplitudes of the release events, and the degree of consistency compared with manual analysis. For a dependable analysis, it is important to keep the experimental conditions constant and to perform the complete analysis with the same threshold *Criteria*.

The amplitudes of the detected events in cat permeabilized ventricular myocytes are slightly smaller than those described before (24), most likely attributable to a higher free Ca concentration in the cytosolic solution (150 nM in the present study vs. 100 nM before), which leads to a smaller normalized amplitude ($\Delta F/F_0$) because of the higher cytosolic fluorescence level. The smaller spark amplitude in permeabilized vs. intact myocytes can be explained by the increased cytosolic Ca buffering capacity due to 0.35 mM EGTA in the cytosolic solution. Additionally, as described before, the high free Ca concentration in the cytosolic solution leads to a reduced peak amplitude.

The ability of SparkMaster to analyze Ca sparks in skeletal muscle is demonstrated in Fig. 6. A threshold *Criteria* = 3.8 was used. As the profiles in Fig. 6D show, the measurements of the full duration can be a valuable index for the duration of long-lasting Ca-release events, especially when a large fraction of the event shows a relatively stable fluorescence below the half maximal fluorescence (Fig. 6D, top). The FDHM would in these cases not adequately describe the prolonged nature of the events.

The results of the kinetic analysis are appropriate most of the time; however, we encourage the user to confirm the results of the automatic analysis for the specific preparations and experimental conditions used. For example, as shown in Fig. 7C, under certain conditions and with special preparations, it might be more accurate to fit the decay of some sparks with the sum of two exponential functions instead of a single exponential function as performed by SparkMaster (6). However, the time constant calculated by SparkMaster is still valuable because the result is close to the fast component of the decay.

In summary, we present here a freely available program for Ca spark analysis in confocal line-scan images. It runs as a plug-in in the freely available image-processing software ImageJ and is optimized for easy usage. The program is able to correctly detect Ca sparks and perform a detailed kinetic analysis in a wide range of cellular preparations and experimental conditions. Because the underlying analysis algorithm is based on the gold standard of spark analyses, results obtained with SparkMaster can be readily compared with analyses performed with the originally described IDL macro. We therefore anticipate that our program will be a valuable tool for scientists studying elementary Ca-release events.

ACKNOWLEDGMENTS

We thank Dr. Vyacheslav M. Shkryl and Dr. Natalia Shirokova, Department of Pharmacology and Physiology, University of Medicine and Dentistry of New Jersey, New Jersey Medical School (Newark, NJ) for spark images of

skeletal muscle. We thank Dr. Maksym Harhun and Dr. Thomas B. Bolton, Department of Basic Medical Sciences/Pharmacology, St. George's Hospital Medical School (London, UK) for spark images of smooth muscle.

GRANTS

This work was supported by National Heart, Lung, and Blood Institute Grants HL-30077 (D. M. Bers), HL-80101 (D. M. Bers and L. A. Blatter), and HL-062231 (L. A. Blatter) and by Grants from the American Heart Association (0550170Z to L. A. Blatter and 0530309Z to A. V. Zima).

REFERENCES

- Baylor SM. Calcium sparks in skeletal muscle fibers. *Cell Calcium* 37: 513–530, 2005.
- Cheng H, Lederer MR, Xiao RP, Gomez AM, Zhou YY, Ziman B, Spurgeon H, Lakatta EG, Lederer WJ. Excitation-contraction coupling in heart: new insights from Ca sparks. *Cell Calcium* 20: 129–140, 1996.
- Cheng H, Lederer WJ, Cannell MB. Calcium sparks: elementary events underlying excitation-contraction coupling in heart muscle. *Science* 262: 740–744, 1993.
- Cheng H, Song LS, Shirokova N, Gonzalez A, Lakatta EG, Rios E, Stern MD. Amplitude distribution of calcium sparks in confocal images: theory and studies with an automatic detection method. *Biophys J* 76: 606–617, 1999.
- Gomez AM, Cheng H, Lederer WJ, Bers DM. Ca diffusion and sarcoplasmic reticulum transport both contribute to [Ca]_i decline during Ca sparks in rat ventricular myocytes. *J Physiol* 496: 575–581, 1996.
- Gordienko DV, Bolton TB. Crosstalk between ryanodine receptors and IP₃ receptors as a factor shaping spontaneous Ca-release events in rabbit portal vein myocytes. *J Physiol* 542: 743–762, 2002.
- Gordienko DV, Greenwood IA, Bolton TB. Direct visualization of sarcoplasmic reticulum regions discharging Ca sparks in vascular myocytes. *Cell Calcium* 29: 13–28, 2001.
- Isaeva EV, Shkryl VM, Shirokova N. Mitochondrial redox state and Ca sparks in permeabilized mammalian skeletal muscle. *J Physiol* 565: 855–872, 2005.
- Izu LT, Wier WG, Balke CW. Theoretical analysis of the Ca spark amplitude distribution. *Biophys J* 75: 1144–1162, 1998.
- Nelson MT, Cheng H, Rubart M, Santana LF, Bonev AD, Knot HJ, Lederer WJ. Relaxation of arterial smooth muscle by calcium sparks. *Science* 270: 633–637, 1995.
- Ouyang K, Zheng H, Qin X, Zhang C, Yang D, Wang X, Wu C, Zhou Z, Cheng H. Ca sparks and secretion in dorsal root ganglion neurons. *Proc Natl Acad Sci USA* 102: 12259–12264, 2005.
- Satoh H, Blatter LA, Bers DM. Effects of [Ca]_i, SR Ca load, and rest on Ca spark frequency in ventricular myocytes. *Am J Physiol Heart Circ Physiol* 272: H657–H668, 1997.
- Satoh H, Katoh H, Velez P, Fill M, Bers DM. Bay K 8644 increases resting Ca spark frequency in ferret ventricular myocytes independent of Ca influx: contrast with caffeine and ryanodine effects. *Circ Res* 83: 1192–1204, 1998.
- Sebille S, Cantereau A, Vandebrouck C, Balghi H, Constantin B, Raymond G, Cognard C. Calcium sparks in muscle cells: interactive procedures for automatic detection and measurements on line-scan confocal images series. *Comput Methods Programs Biomed* 77: 57–70, 2005.
- Shkryl VM, Shirokova N. Transfer and tunneling of Ca from sarcoplasmic reticulum to mitochondria in skeletal muscle. *J Biol Chem* 281: 1547–1554, 2006.
- Song LS, Sham JS, Stern MD, Lakatta EG, Cheng H. Direct measurement of SR release flux by tracking “Ca spikes” in rat cardiac myocytes. *J Physiol* 512: 677–691, 1998.
- Song LS, Stern MD, Lakatta EG, Cheng H. Partial depletion of sarcoplasmic reticulum calcium does not prevent calcium sparks in rat ventricular myocytes. *J Physiol* 505: 665–675, 1997.
- Terentyev D, Viatchenko-Karpinski S, Valdivia HH, Escobar AL, Gyorke S. Luminal Ca controls termination and refractory behavior of Ca-induced Ca release in cardiac myocytes. *Circ Res* 91: 414–420, 2002.
- Tsugorka A, Rios E, Blatter LA. Imaging elementary events of calcium release in skeletal muscle cells. *Science* 269: 1723–1726, 1995.
- Wier WG, ter Keurs HE, Marban E, Gao WD, Balke CW. Ca “sparks” and waves in intact ventricular muscle resolved by confocal imaging. *Circ Res* 81: 462–469, 1997.
- Yang Z, Steele DS. Characteristics of prolonged Ca release events associated with the nuclei in adult cardiac myocytes. *Circ Res* 96: 82–90, 2005.
- Zhou J, Brum G, Gonzalez A, Launikonis BS, Stern MD, Rios E. Ca sparks and embers of mammalian muscle. Properties of the sources. *J Gen Physiol* 122: 95–114, 2003.
- Zima AV, Blatter LA. Sarcoplasmic reticulum Ca load controls duration and termination of Ca sparks in cardiac myocytes (Abstract). *Biophys J* 90: 2006.
- Zima AV, Kockskamper J, Blatter LA. Cytosolic energy reserves determine the effect of glycolytic sugar phosphates on sarcoplasmic reticulum Ca release in cat ventricular myocytes. *J Physiol* 577: 281–293, 2006.
- Zima AV, Kockskamper J, Mejia-Alvarez R, Blatter LA. Pyruvate modulates cardiac sarcoplasmic reticulum Ca release in rats via mitochondria-dependent and -independent mechanisms. *J Physiol* 550: 765–783, 2003.